Single-Layered Frequency Selective Surface for Polarization Processing by Transmission Through Elementary Simple Structure Unit Cell Array

Received January 5, 2021, accepted February 15, 2021, date of publication February 18, 2021, date of current version February 26, 2021.

Digital Object Identifier 10.1109/ACCESS.2021.3060155

Single-Layered Frequency Selective Surface for Polarization Processing by Transmission Through Elementary Simple Structure Unit Cell Array

ANDREI-MARIUS SILAGHI[1], (Student Member, IEEE), ALDO DE SABATA[1], (Member, IEEE), AND LADISLAU MATEKOVITS[1,2,3], (Senior Member, IEEE)

[1]Department of Measurements and Optical Electronics, University Politehnica Timisoara, 300006 Timisoara, Romania
[2]Dipartimento di Elettronica e Telecomunicazioni, Politecnico di Torino, 10129 Turin, Italy
[3]Instituto di Elettronica e di Ingegneria dell'Informazione e delle Telecomunicazioni, National Research Council of Italy, 10129 Turin, Italy

Corresponding author: Ladislau Matekovits (ladislau.matekovits@polito.it)

This work was supported by the Ministry of Education and Research of Romania through UEFISCDI, under Project PN-III-P1-1.2-PCCDI-2017-0917.

ABSTRACT A single metal layer, multifunctional frequency selective surface with a very simple pattern of the unit cell, containing a U-shaped metal resonator on FR4 substrate, and working in the low GHz frequency range is proposed. The structure realizes dual linear polarization filtering at frequencies of 1.83 and 4.14 GHz with fractional bandwidths of 34.15% and 22.51% respectively, and linear-to-circular polarization conversion at 2.68 GHz, with 3.2 dB insertion loss (IL), 30-45° angular stability depending on the direction of arrival of the incident wave, and 22.01% axial ratio bandwidth. The dimension of the unit cell corresponds to 0.09, 0.13 and 0.21 fractions of wavelength at the three operational frequencies. The functionality of the proposed structure is assessed by simulation, circuital model, and experiment in anechoic chamber. Scalability is demonstrated by designs that work at different frequencies, tested by simulation.

INDEX TERMS Frequency selective surface (FSS), notch filter, angular stability, polarization filtering and conversion.

I. INTRODUCTION

Polarization processing of waves has been a research subject of interest in the last years [1]. Practical aspects focused researchers' attention on processing of linear (LP) and circularly polarized (CP) waves. LP filtering involves leaving unaffected the co-polarization component of a plane wave and filtering out the cross-polarization part [2]. Linear-to-circular polarization conversion (LCPC) is another subject of wide interest. CP waves have important applications in modern communications systems and sensor networks due to an increased insensitivity to propagation effects such as multipath fading, reflections, Faraday effect in the Ionosphere etc. An effective way of obtaining CP plane waves relies on frequency selective surfaces (FSSs) that realizes an LCPC. FSSs are 2D periodic surfaces that result from translation of a basic spatial element, called unit cell, in two independent directions. The most common arrangement consists of translations in a plane along two orthogonal lines [3]. When FSSs are used for filtering or selective screening, insensitivity to polarization is a desirable effect and therefore several axes of symmetry are considered in the design of the surface. When polarization processing is targeted, waves must propagate through an anisotropic medium, so that the number of symmetries exhibited by the surface must be reduced.

An early linear-to-circular polarizer based on meander metallic lines on a surface has been reported in [4]. The polarizer has been realized both in planar and cylindrical form. However, the proper operation of the polarizer involved several layers in its construction, making it bulky for applications [2].

Multiple-layer LP-CP converters have been considered by many authors. In [5], a polarizing structure that reflects LP waves as CP waves at one frequency and is transparent at other frequencies is proposed. The structure consists of two parallel surfaces with unit cells based on dipoles. The dipoles on one surface are placed orthogonally with respect of the dipoles on the other surface.

A dual-band LP-CP converter is proposed in [6], which converts LP incident waves in right circularly

The associate editor coordinating the review of this manuscript and approving it for publication was Jun Shen.

polarized (RCP) or left circularly polarized (LCP) transmitted waves depending on the frequency (of the wave). The design of the unit cell involves three metallic layers composed of metallic patches, a split ring, and a circular slot. The structure is designed to operate in the K/Ka satellite communication band.

In [7], a dual band LP-CP converter is considered, based on a four-metal layer structure separated by dielectric layers. Unit cells contain split-ring resonators bisected by metal strips and rectangular patches and rings. The polarizer operates in the 6.4 - 8.8 GHz and 12.1 - 13.9 GHz bands.

FSS depending on slot-line based unit cells arranged in two orthogonal directions in a multi-layer 3D structure has been conceived, designed, and demonstrated to operate as a polarization converter, covering the X band [8]. Two identical metal layers with patterns consisting of a Jerusalem cross and linear dipoles have been placed on a separating dielectric layer to obtain a dual band polarization converter working in the K/Ka band [9].

A bilayer-twisted Fermat's spiral chiral metamaterial is proposed for the realization of circular polarization of far-infrared waves and polarization filters in [1]. It is demonstrated that the proposed structure can convert waves from linear to circular polarization around 2.5 THz.

A tunable converter working in the terahertz frequency range and consisting of two layers of metal and graphene resonators, respectively, separated by a dielectric layer has been reported [10]. The tunability is provided by the possibility of controlling the Fermi energy of the graphene material.

A physics perspective on polarization processing and various applications using multi-layered surfaces from GHz to THz, as well as important references can be found, for example, in the review article [11].

The literature reporting various structures based on multiple-layer FSS polarizers is extensive. Some recent publications are [12]–[18]. Other titles can be found as references in the cited literature.

Besides multiple-layer FSSs, single-layer solutions, consisting of a metal pattern on top of a thin dielectric slab, have also been proposed.

A single metal layer LP-CP converter based on a sub-millimeter cross-slot unit cell and another single layer converter based on ring slots on a dielectric layer have been introduced in [19]. IL of 3.2-3.3 dB at the operation frequency of 325 GHz, and 3 dB axial ratio (AR) fractional bandwidths of 17.3% and 20.4% have been obtained for the two designs, respectively. The cross-slot metallic pattern has been replicated on the other side of the dielectric layer. The obtained two-metal layer design featured a better IL than in the single-layer case (0.55 dB) and a fractional AR bandwidth of 12.2%.

It is well known that using multiple layers enhances desired properties of FSSs, such as bandwidth and IL [3]. However, from a feasibility point of view, it is desirable to use thin structures, which also reduces attenuation and multiple reflection of waves that otherwise propagate through successive metal and dielectric layers.

A single-layer variation of the metallic meander line in combination with a loop configuration has been proposed in [2] to achieve a LP-CP conversion with an AR below 3 dB in the range 18-20 GHz (46.8%) and IL between 2.5 and 3 dB, for a dimension of the unit cell of 23.5 mm. The structure has been proven to operate properly up to an angle of incidence of 30°.

A broadband LP-CP converter made of a layer of zig-zag metal strips on a dielectric substrate has been reported in [20]. A 3 dB AR bandwidth of 53% has been achieved experimentally (and 70.5% in theory) in the 6-12 GHz band, with a unit cell of 6×6 mm. The broadband operation has been obtained by avoiding the resonant character of the unit cell that is relied upon in other implementations of polarizers. The structure has been tested to incident angles up to 30°.

A single layer, dual band polarization converter has been proposed in [21]. It provides opposite circular polarization for incident linear polarization in the Ku band (17.2 GHz) and Ka band (34.2 GHz), with AR bandwidth of 21% and angular stability of 45° and 30° respectively. The edge of the square-shaped of the unit cell is 5.2 mm (0.3 λ). The metal pattern consisting of a split ring is surrounded by a closed square ring.

Considering the wide interest on the topic, in this article, we focus on a cost-effective, easy-to-fabricate, scalable single-layer metal-on-dielectric polarization processing surface.

In this article we report a multi-functional FSS that realizes the following polarization processing operations:

- it filters out LP waves along one direction while it does not affect LP waves over an orthogonal direction (the cross-pol component) at one frequency;
- it realizes the complementary operation (i.e., transmits LP waves along the first direction and filters out LP waves along the orthogonal direction) at another frequency;
- it converts LP waves along directions making an angle of $\pm 45°$ with the previous directions to CP waves at an intermediary frequency.

The structure of the unit cell we considered is of elementary simplicity, relying on a U-shaped metal resonator over a thin dielectric layer.

U-shaped metal patterns for square shaped FSS unit cells have already been considered by several authors. In [22], transmittance of FSSs having unit cells with single and double U-shaped patterns are considered in view of absorber and sensor applications. Additionally, a quad super-cell, consisting of four rotated U-shaped cells is designed in view of providing symmetry to the structure. Anisotropy is demonstrated in the first two cases. However, polarization conversion applications are not considered in that article.

In an older reference [23], nested U-shaped metal patterns on dielectric are introduced and assessed to react in the X band. However, the focus is on metamaterial-related

parameters of the structure rather than polarization conversion.

Double-layer, quad rotated U-shaped resonators have also been used in the past for devising chiral metamaterials with negative refractive index [24].

A double metal layer using quad super-cells consisting of rotated and scaled U-shaped resonator has been reported in [25]. Dual-band polarization conversion has been demonstrated in the 3-7 GHz frequency range. However, investigations concerning AR bandwidth, IL and response to oblique incidence have not been reported.

The rest of the article is organized as follows. In Section II, we present the proposed structure, its operation principle and its transmission characteristics obtained by full-wave simulation. In Section III, we report an equivalent circuit for the structure. Experimental results on large extension prototype are presented in Section IV, and compared with numerical simulation obtained data. Conclusions are drawn in the last section.

II. UNIT CELL STRUCTURE AND SIMULATION RESULTS

The front view of the unit cell of the proposed structure is presented in Fig. 1 (a) and a CAD model is reported in Fig. 1 (b).

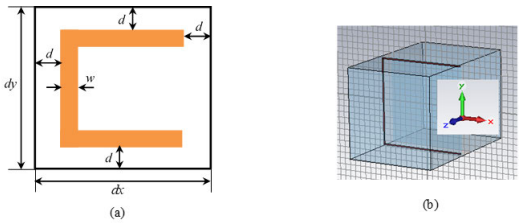

FIGURE 1. Unit cell: front view with relevant dimensions indicated (a); CAD model (with hidden dielectric layer for a better rendering) (b).

The periodic surface is built on an FR4 substrate ($\varepsilon_r = 4.3$, $\tan(\delta) = 0.025$), having a thickness of 2.4 mm. At the considered frequency range, the value of the thickness has reduced influence on the response of the surface to incoming electromagnetic waves due to the short path of the waves through the dielectric. The U-shaped metal pattern has equal arms, situated at equal distance d from all the the bounds of the unit cell. This parameter is technologically important since $D = 2d$ is the distance between adjacent metal traces (that will be indicated below instead of d). An equally important parameter is the trace width w.

The dimensions for the structure that we used in simulations have been $dx = dy = 15$ mm, $w = 0.2$ mm and $D = 0.4$ mm. Simulations have been carried out by means of a commercial solver [**?**], by illuminating the surface with linearly polarized waves incident on the patterned face. The transmittance (magnitude of the transmission coefficient) of the surface is reported in Fig. 2 (a). The curve labelled as "Case 1" corresponds to E-field parallel to the y axis, while "Case 2" relates to E-field parallel to the x axis, with respect to the coordinate system in Fig 1 (b). We will denote by T_1

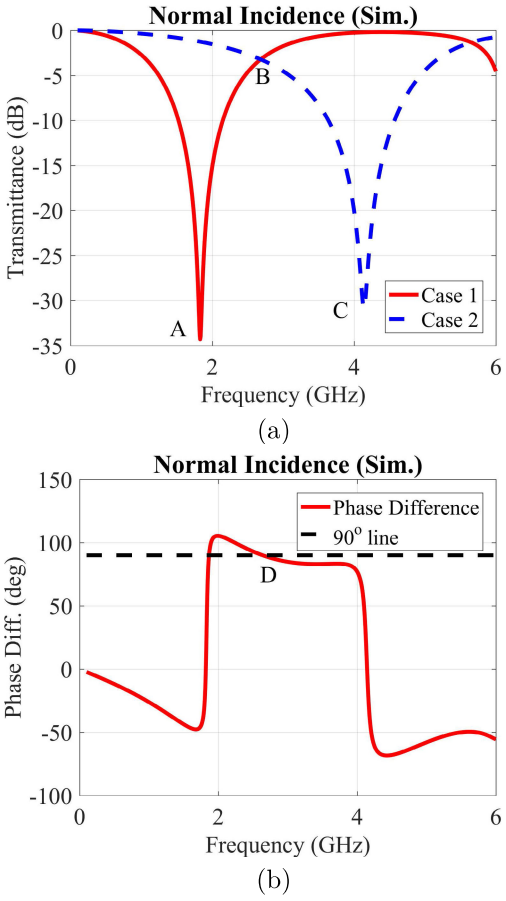

FIGURE 2. Transmission coefficient: magnitude (a); phase difference at the output between in-phase, orthogonally polarized waves at the input (b).

and T_2 respectively the transmittance in the two cases. The phase difference acquired by two linearly polarized waves according to Case 1 and Case 2 respectively, upon passing through the surface, is represented in Fig. 2 (b).

There are three interesting points on the graphs in Fig. 2 (a). At point A, corresponding to a frequency $f_1 = 1.83$ GHz, y-polarized waves (Case 1) are strongly attenuated ($T_1 = -34.29$ dB, with a relative -10 dB bandwidth of 34.15%), while x-polarized waves (Case 2) are attenuated by only -1.26 dB. This means that, in the case of mixed input polarization, the output will be x-polarized, i.e., linearly polarized transmitted field, independently of the polarization of the incident field.

At point C, corresponding to a frequency $f_3 = 4.14$ GHz, the same holds for the orthogonally polarized component since $T_1 = -0.22$ dB and $T_2 = -30.84$ dB (with a relative -10 dB bandwidth of 22.51%). Any elliptically polarized wave at the input will be y-polarized at the output.

The transmittances are equal at point B, $T_1 = T_2 = -3.24$ dB, at a frequency $f_2 = 2.68$ GHz. At this frequency, the phase difference is very close to 90° (approximately 89.34°, point D in Fig. 2 (b)). Consequently, an LP wave at 45° with respect to the x axis (Fig. 1 (b)) at the

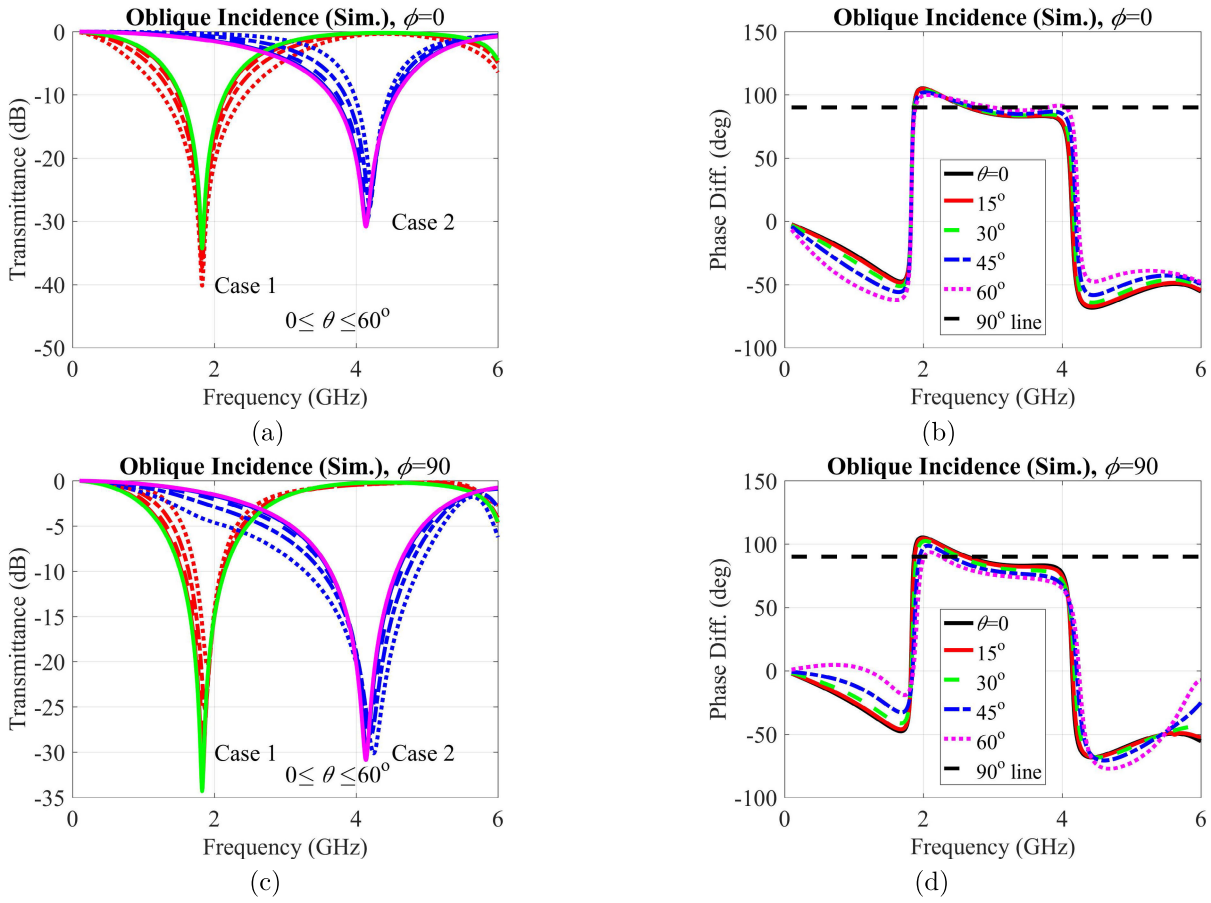

FIGURE 3. Oblique incidence: (a) transmittance $\phi = 0$ (normal incidence – solid line); (b) phase difference $\phi = 0$; (c) transmittance $\phi = 90°$ (normal incidence – solid line); (d) phase difference $\phi = 90°$.

input will be RCP at the output, while an LP wave at 135° at the input will be LCP at the output. Indeed, the x and y input E-field amplitudes are equal in both cases, while the phases are equal in the first case and in opposition (180° difference) in the second case. At the output, the amplitudes are still equal, but the y component is advanced by 90° with respect to input. The phase difference between the y and x components determines the circular polarization and the sense of rotation at the output, considering waves propagating along the negative z axis [26].

In a practical installation of a polarization-processing device, it is important to allow a certain degree of misalignment with respect to the axis determined by the emitting and receiving antennas. Thus, we have tested the proposed structure to oblique incidence with respect to the xOy plane in Fig. 1 (b). We denote by θ and ϕ the co-latitude and azimuth angles associated to the reference frame $Oxyz$. Since the structure is anisotropic, we have determined by simulation the transmittance parameters for a range of θ from 0 to 60°, with a step of 15°, for both $\phi = 0$ and $\phi = 90°$. The transmittance and phase difference for $\phi = 0$ are reported in Fig. 3 (a) and (b) respectively, and the same quantities for $\phi = 90°$ are represented in Fig. 3 (c) and (d).

The results reported in Fig. 3 indicate that the polarization filtering properties of the proposed FSS possess a good stability in the considered range of incidence angles. Also, the phase difference is stable at the frequency of interest (2.68 GHz). However, the capability of providing a proper CP outgoing wave requires special consideration.

The geometrical locus of the tip of the electric field intensity vector at 2.68 GHz, in a plane perpendicular to the direction of propagation at the output of the polarizer, assuming an input LP wave at 45° with respecte to the x axis of the reference frame in Fig. 1 (b) and with an amplitude of the electric field intensity of 1.41 V/m is represented in Fig. 4 (a) and (b) for the considered angles defining the co-latitude and the azimuth.

To assess the quality of the polarizer, we adopt the widely accepted criterion of AR (ratio of major to minor axes of the polarization ellipse) being smaller than 3 dB. Calculation formulas for the AR and tilt angle in function of the x and y components of the wave are widely available, thus we do not reproduce them here (see e.g. [26]).

It turns out that, for $\phi = 0$, the AR is 1.45 dB for $\theta = 30°$ and 3.31 dB for $\theta = 45°$. If $\phi = 90°$, the AR is 2.28 dB for $\theta = 45°$ and 4.67 dB for $\theta = 60°$. Therefore, the polarizer has

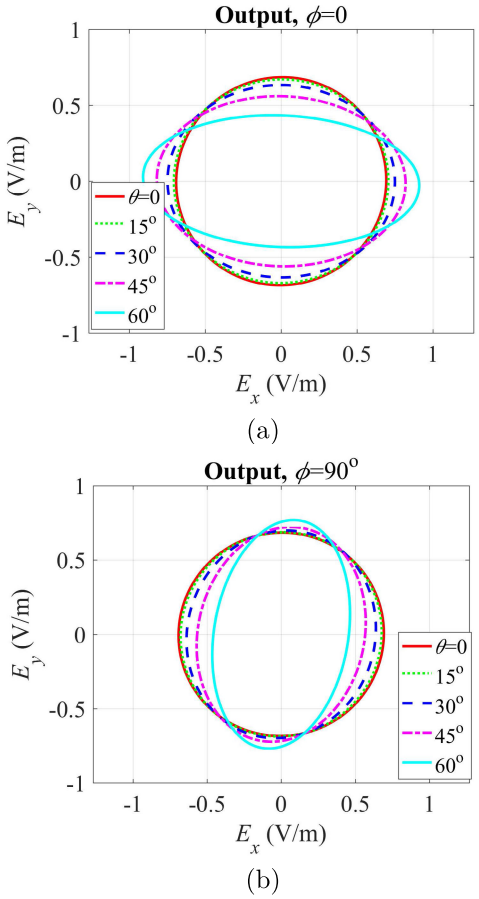

FIGURE 4. Polarization ellipse at the output of the polarizer for a 45° LP incident wave parametrized after θ, for $\phi = 0$ (a) and $\phi = 90°$ (b). Amplitude of the incident wave is considered to be equal to 1.41 V/m.

a demonstrated AR below 3 dB for incidence margins given by $\theta \leq 30°$, $\phi = 0$, and $\theta \leq 45°$, $\phi = 90°$. The minimum AR, at the operation frequency, is 0.14 dB, and is obtained for normal incidence.

It is noted that for the $\phi = 0$ case, the ellipses maintain the principal axis at small angles with the x and y directions, while for the $\phi = 90°$ there is a rotation off them. This behavior is due to the different symmetries the structure possesses with respect to the two coordinate axis in the xOy plane. There is a symmetry of the structure with respect to the x axes, that is in turn broken for the orthogonal y direction. In this second case, the effect is even more pronounced when the incidence angle increases, since the projections of the incident field on the asymmetric arms increases, hence the scattering of the cross term increases.

Another important feature of the polarizer is the dependency of the AR on frequency for normal incidence. This behavior is represented in Fig. 5. The band limits corresponding to an AR below 3 dB are 2.43 GHz and 3.02 GHz, resulting, with respect to the operating frequency of 2.68 GHz, a relative bandwidth of 22.01%.

Several simulations have been performed to assess the coverage of frequency range up to 15 GHz by stretching the

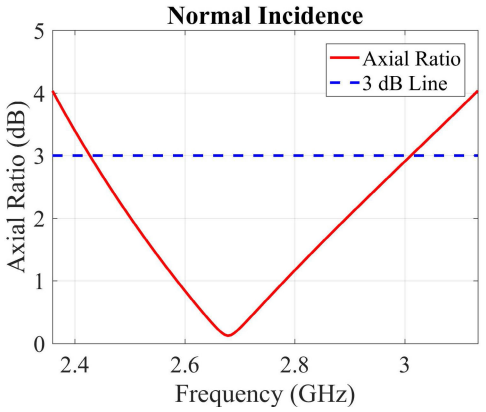

FIGURE 5. Axial ratio vs. frequency (only the frequency band of interest is reported).

structure. Simply scaling down was not possible motivated by technological constraints on trace width. We have scaled down the dimensions of the unit cells and used the parameters D and w to optimize the structure to have a phase difference of 90° at f_2, where the x and y transmittances are equal. The dimensions are listed in Tab. 1 and the relevant transmission coefficient parameters in Tab. 2. Supplementary to the parameters f_i and T_i, the -10 dB bandwidths B_1 and B_3 around f_1 and f_3 respectively and the computed phase difference $\Delta\Phi$ at f_2 are provided. The -10 dB bandwidth is largely accepted as a relevant parameter in FSS's [27].

TABLE 1. Scaled Down Geometrical Dimensions

Cases	$dx = dy$ (mm)	w (mm)	D (mm)
1	15	0.2	0.35
2	12.5	0.2	0.6
3	10	0.2	0.65
4	7.5	0.2	0.8
5	5	0.2	0.55

Having presented the main operational features of the proposed FSS, we now consider in the next section an explanation of its behavior by means of a circuital model.

III. CIRCUIT MODEL

It is known that LP waves incident on an array of parallel strips experience an inductive effect when the E-field is parallel to the strips and a capacitive one when the E-field is perpendicular to the strips [3]. In our case, we have a combination of parallel and perpendicular dipoles, and therefore a combination of the two effects is expected. Since we have single dipoles parallel to the y axis and closely spaced dipoles parallel to the x axis (considering several unit cells as in Fig. 1 (a)), we expect a larger inductance for LP waves parallel to the y axis than in the other case. The closely spaced dipoles are expected to introduce a strong capacitive effect for LP waves parallel to the y axis, while the capacitive effect introduced by the closely spaced, parallel dipoles is expected to be weaker when waves are LP along the x axis.

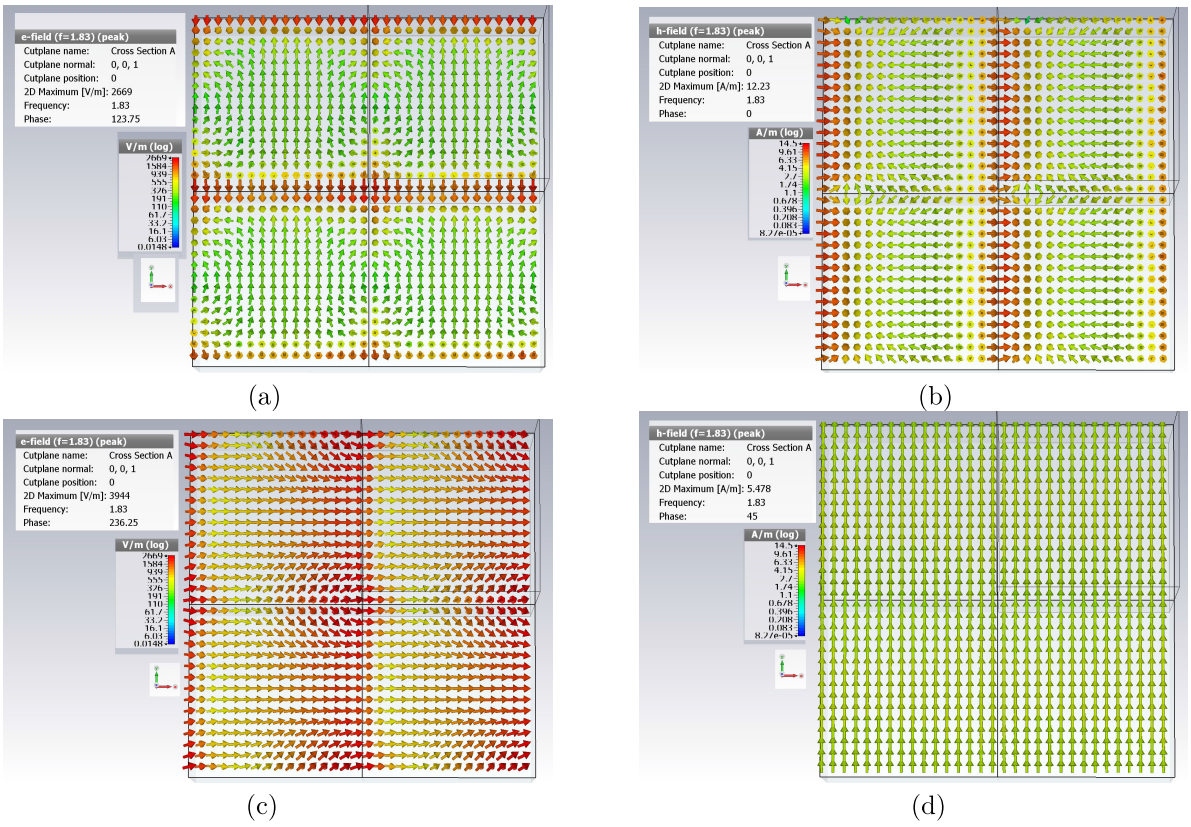

FIGURE 6. Field images at 1.83 GHz (a) E- field, Case 1; (b) H-field, Case 1; (c) E- field, Case 2; (d) H-field, Case 2.

TABLE 2. Transmission Parameters for the Structures With Unit Cells Defined by Dimensions in Tab. 1

Cases	f_1 (GHz) T_1 (dB) T_2 (dB) B_1 (GHz)	f_2 (GHz) $T_1 = T_2$ (dB) $\Delta\Phi$ (°)	f_3 (GHz) T_1 (dB) T_2 (dB) B_3 (GHz)
1	1.81 -35.09 -1.33 0.68	2.67 -3.24 89.6	4.1 -0.28 -31.38 0.98
2	2.32 -33.52 -1.6 0.73	3.3 -3.31 89.9	5.22 -0.25 -31.3 1.25
3	3.16 -32.55 -1.96 0.89	4.17 -3.45 90.9	6.8 -0.52 -30.4 1.52
4	4.64 -31.28 -2.48 1.13	5.76 -3.59 91.6	9.81 -1.37 -28.85 1.93
5	7.12 -31.06 -3.16 1.74	8.55 -3.98 90.6	15.13 -2.38 -27.61 2.85

Note: the values of f_2 and $\Delta\Phi$ have been calculated by sweeping 1 GHz around, at a required precision of 1e-12 (CST 2020 Frequency Domain Solver). For the rest, the scan has been 10 GHz wide with 1e-9 accuracy.

These arguments explain the two resonant frequencies that are polarization dependent in Fig. 2 (a).

To get insight into the origin of the capacitive and inductive effects, we consider the field images in Figs. 6 and 7.

The field images in Fig. 6 (a) and (b) represent the electric and magnetic field intensities respectively, at 1.83 GHz for Case 1 (E-field parallel to the *y* axis, i.e., vertical). The E-field intensity in Fig. 6 (a) reveals a strong capacitive effect in the region of the closely spaced horizontal dipoles, as expected. Also, in the region of the vertical dipoles, we have a typical image of a dipole near field, which enhances the capacitive effect of the structure at the considered frequency. The H-field image in Fig. 6 (b) reveals a concentration of the magnetic field in the region of the vertical dipoles, indicating an inductive contribution of these dipoles. The magnetic field intensity is weak in the region of the horizontal dipoles. These conclusions are supported by the surface current images (not reported here). The surface current has high values on the vertical dipoles but opposite directions, cancelling any inductive effect, along the horizontal dipoles. The combination of *LC* elements explains the first resonance in Fig. 2 (a) (point A, Case 1).

The field images in Fig. 6 (c) and (d) represent the electric and magnetic field intensities respectively, at 1.83 GHz for Case 2. A capacitive effect exists between horizontal dipoles and vertical ones, as revealed by Fig. 6 (c). This explains the small drop of 1.26 dB in the transmission coefficient for this polarization at 1.83 GHz. The structure has little effect on the H-field, which remains uniform and vertically polarized,

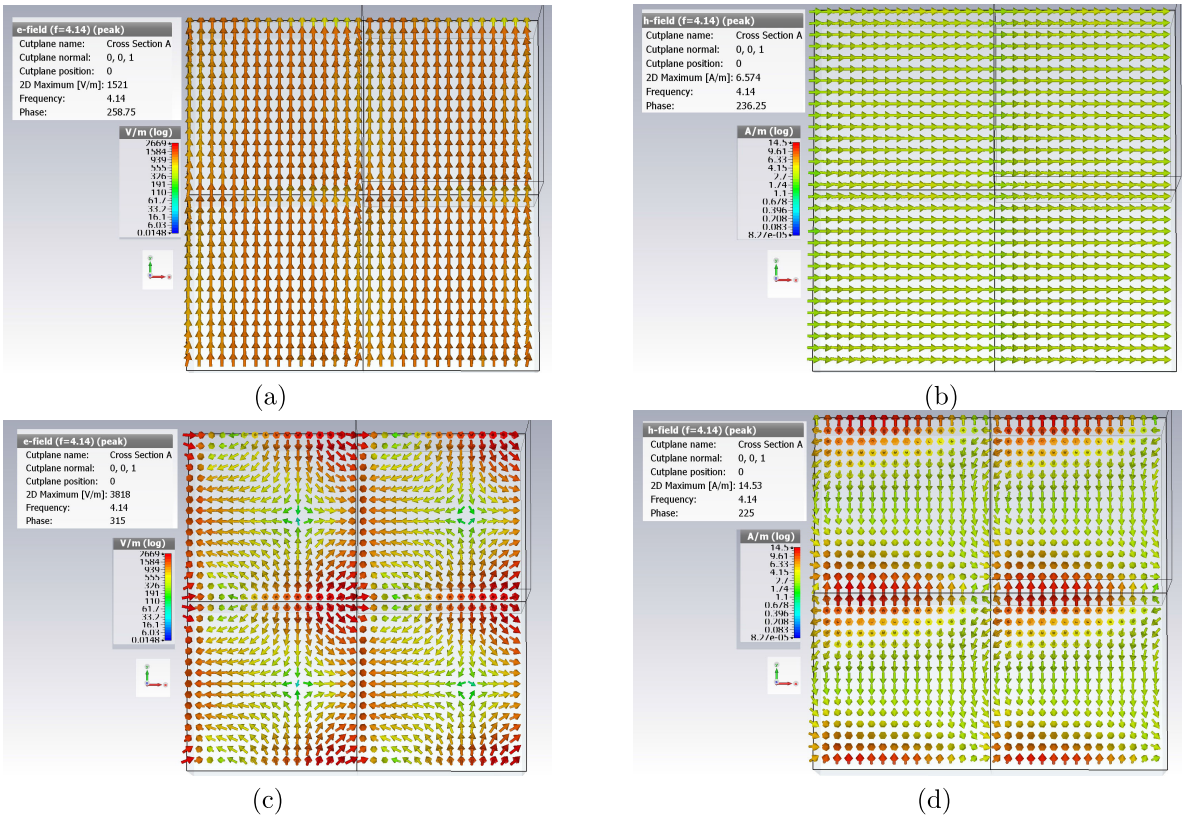

FIGURE 7. Field images at 4.14 GHz (a) E- field, Case 1; (b) H-field, Case 1; (c) E- field, Case 2; (d) H-field, Case 2.

like in the incident wave, as seen in Fig. 6 (d). In conclusion, the structure is resonant at 1.83 GHz for vertically polarized LP waves and out of resonance for horizontally polarized ones.

The field images in Fig. 7 reveal a different response of the structure to incoming LP waves at 4.14 GHz. The E-field for Case 1, corresponding to vertically polarized LP waves, is reported in Fig. 7 (a). The field is slightly perturbed around the conductors, due to the capacitive interaction between the vertical and the horizontal dipoles. The H-field passes through the structure practically unperturbed, as shown in Fig. 7 (b). Overall, the interaction between LP waves and the FSS is very weak in Case 1, which explains the small attenuation of 0.22 dB. The situation is different in Case 2, when incoming LP waves are horizontally polarized. A strong capacitive coupling between vertical and horizontal dipoles is present, as revealed by the image of the E-field in Fig. 7 (c). The H-field, reported in Fig. 7 (d) circles around the pair of closely spaced horizontal dipoles, which introduces an inductive effect. This combination of LC elements explains the notch at 4.14 GHz for Case 2 (point C in Fig. 2 (a)).

The capacitance for Case 1 at 1.83 GHz includes the contribution of the closely spaced, parallel horizontal dipoles and is therefore larger that the capacitance for Case 2 at 4.14 GHz, which relies on the interaction between

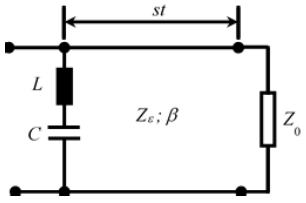

FIGURE 8. Equivalent circuit of the unit cell.

perpendicular dipoles. The inductance for Case 1 at 1.83 GHz corresponds to a metal strip (Fig. 6 (b)). However, some field non-uniformities are present at the ends of the strip, so that some corrections will be necessary if a formula for a finite length metal strip will be applied. It is tempting to say that the inductance for Case 2 at 4.14 GHz is half of the inductance for Case 1, since two identical parallel metal strips are circled by the magnetic field intensity vector. However, the field is not uniform along the length of the strips, as seen on (Fig. 7 (d)) and consequently only a fraction of the length of the dipoles determines the value of the equivalent inductance. The above presented discussion suggests the equivalent circuit for the unit cell of the FSS presented in Fig. 8.

The equivalent circuit consists of the LC elements introduced in connection to the field images of Figs. 6 and 7, a length of transmission line equal to the FR4 substrate

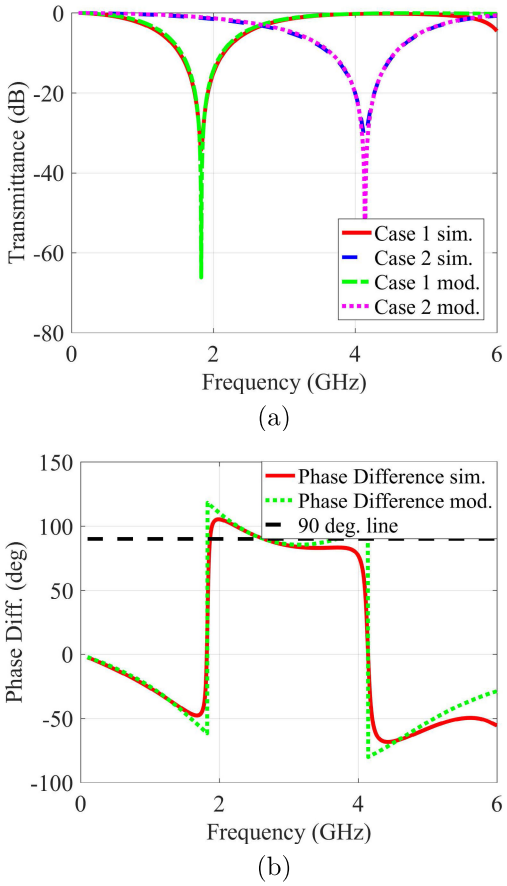

FIGURE 9. Transmission coefficient obtained by simulation (sim.) and circuit model (mod.): (a) magnitudes; (b) phase difference.

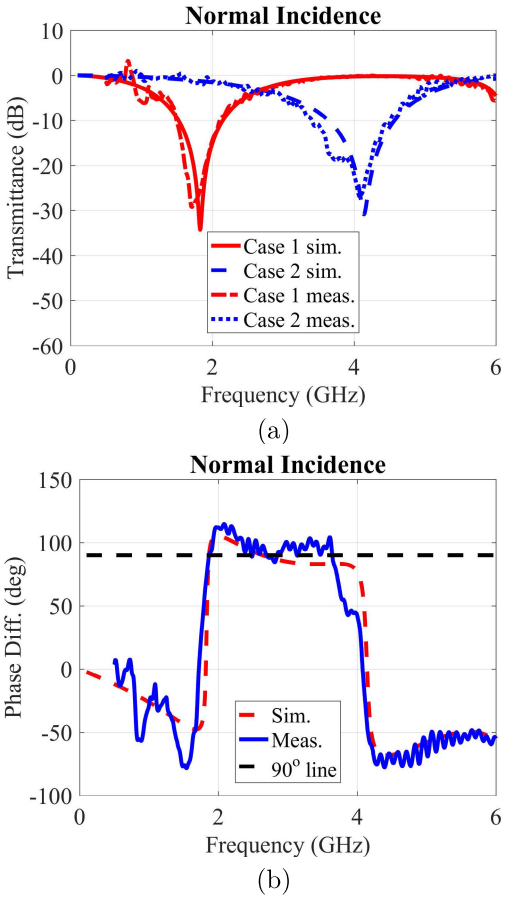

FIGURE 11. Transmission coefficient in normal incidence, measured vs simulated: (a) magnitude; (b) phase difference.

FIGURE 10. Experimental equipment: (a) Fabricated finite sized FSS on PCB and emitting antenna in anechoic chamber; (b) receiving antenna.

thickness st, having the characteristic impedance Z_ε and a propagation constant β corresponding to the dielectric constant of the substrate and terminated by a load impedance equal to the free-space impedance. The circuit is fed by a matched generator of internal impedance Z_0 (not represented), accounting for the incident wave propagating through free space. The equivalent circuit is different for Case 1 than for Case 2, due to the lack of symmetry of the structure.

To find the LC elements, we start from a well-known formula for the inductance L of a strip of length s and width w, immersed in a non-magnetic material, for the case of a negligible thickness [28]:

$$L = \mu_0 \frac{s}{2\pi} \ln\left(\frac{2s}{w}\right) \tag{1}$$

Since the capacitive effects are multiple, we calculate the capacitance from the known resonance frequency f_r according to

$$f_r = \frac{1}{2\pi\sqrt{LC}} \tag{2}$$

By substituting the geometrical parameters of the dipoles reported in Section II into (1), we get an initial value for the inductance in Case 1 of $L_0 = 14.552$ nH. We performed an optimization by starting from this value of the inductance and by applying (2) to find the equivalent capacitance for Case 1. For Case 2, the optimization started from one half of the value of L_0. The transmission coefficient of the circuit in Fig. 8 (S_{21}) has been calculated analytically and implemented in Matlab. The optimization goal was to achieve a transmittance of the circuit as close as possible to the transmittance of the structure obtained by simulation. The following values have been obtained to provide an acceptable match: for Case 1, $L_1 = 16.880$ nH, $C_1 = 0.448$ pF, and for Case 2: $L_2 = 10.186$ nH, $C_2 = 0.145$ pF.

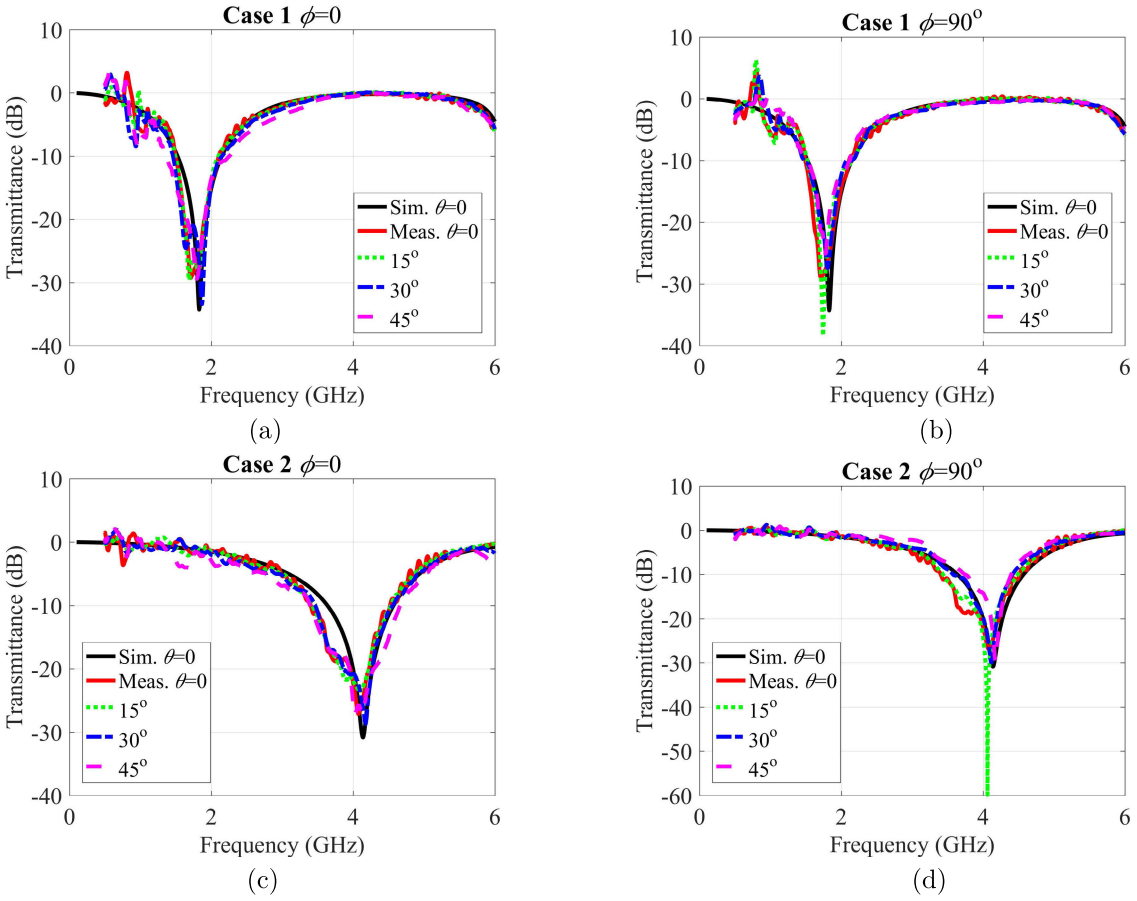

FIGURE 12. Transmittance in oblique incidence for various values of θ. (a) Case 1, $\phi = 0$; (b) Case 1, $\phi = 90°$; (c) Case 2, $\phi = 0$; (d) Case 2, $\phi = 90°$. Results obtained by simulation in normal incidence are also reported for reference.

The transmission coefficients obtained by full-wave simulation and by applying the circuit model are reported jointly in Fig. 9.

The results reported in Fig. 9 show that the circuit model captures the most relevant features of the structure in the frequency range of interest. We have a good match of the transmittance and phase difference, which, moreover, has the correct value of 90° at 2.68 GHz, when the transmittance for Case 1 is equal to the one for Case 2, allowing for the LP-CP conversion.

IV. EXPERIMENTAL VALIDATION

A finite version of the FSS introduced in Section II has been realized and tested experimentally on an FR4 board, of thickness 2.4 mm, comprising 30 × 30 unit cells. A photograph of the structure is reported in Fig. 10 (a), mounted on a screen separating the emitting and receiving antennas in an anechoic room. Fig. 10 (b) displays the receiving antenna in the same anechoic room and the back of the screen (the emitting antenna is also visible).

The structure has been tested in an anechoic room by the substitution method, using the same equipment as described in [29]. The description of the equipment and measurement procedure will be not repeated here.

The experimental results obtained for normal incidence of LP waves are reported in Fig. 11, jointly with the simulation results, to facilitate the comparison. A good match is revealed, both for the notch frequencies and the phase difference. The artefacts present in the measured results are associated to the finite dimensions of the experimental printed circuit board (PCB) and the technological irregularities [29].

The structure has also been tested in oblique incidence, for the following angles in spherical coordinates: co-latitude θ between 0 and 45°, with step of 15°, and azimuth ϕ equal to 0 and to 90°, to assess the simulation results reported in Fig. 3. The experimental setup did not allow an incidence angle of 60°, which was considered in Fig. 3. Nevertheless, the LP-CP conversion has been proved to be performed up to 45°. The correct operation of the structure as a linear polarizer at 1.83 GHz and 4.14 GHz at an angle of incidence of 60° is demonstrated only by simulation. The measured magnitude of the transmission coefficient in oblique incidence is represented in Fig. 12. The transmittance obtained by simulation in normal incidence is also reported for reference.

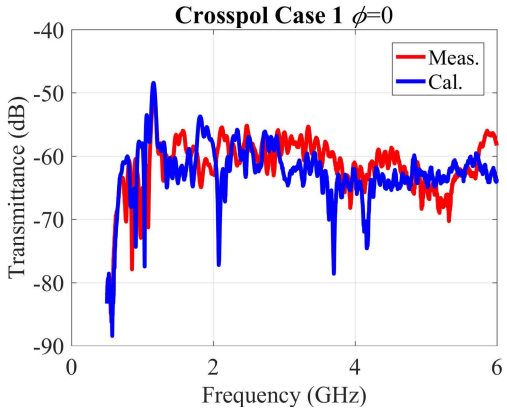

FIGURE 13. Cross-pol transmittance for Case 1, at $\phi = 0$.

Cross-pol components have also been measured, by arranging emitting and receiving antennas at 90°. The measured values have been below −45 dB in all cases. An example is reported in Fig. 13.

The experimental results are in good agreement with the results obtained by simulation, demonstrating the correct operation of the proposed structure.

V. CONCLUSION

A multi-functional single-layer FSS capable of LP filtering at two frequencies with small IL and achieving LP-CP conversion at an intermediary frequency and working in the low GHz frequency range (below 6 GHz, the 5G frequency band) has been introduced. The ratio of the size of the unit cell over operating free space wavelength is 0.09 and 0.21 at the LP filtering frequencies and 0.13 at the polarization conversion frequency. The main parameters of the proposed single metal layer LP-CP converter are as follows: 2.68 GHz working frequency, 3.2 dB IL, 30-45° angular stability depending on the direction of arrival of the incident wave and 22.01% AR bandwidth. The parameters for the structure proposed in [19], which works at much higher frequency – 325 GHz, are: IL = 3.2-3.3 dB, and AR of 17.3% or 20.4%, depending on the design. The converter reported in [2] works in the 6-12 GHz band with an IL of 2.5-3 dB, a 53% AR bandwidth, and an angular stability of 30o. The more recent work [21] introduces a structure with dual-band polarization conversion at 17.2 GHz and 34.2 GHz, with 45° and 30° angular stability respectively, and 21% AR bandwidth (IL not readily available).

The polarization converter proposed in this work has comparable or better parameters than those reported in literature, except for the AR bandwidth of [2], which is superior. However, the proposed structure features multi-functionality by dual LP filtering on one hand, and better feasibility due to the simple structure of the unit cell, based on elementary U-shaped resonators and cost effective FR4 substrate on the other hand.

The LP filters have operation frequencies of 1.83 and 4.14 GHz with relative bandwidths of 34.15% and 22.51% respectively.

The operation principle of the FSS has been elucidated by means of a circuital model.

The functionality of the proposed structure has been demonstrated by simulation and experiment. The scalability of the design by adapting the dimensions of the unit cell and metal pattern, covering the frequency range from 1.81 to 15.13 GHz has also been exemplified.

REFERENCES

[1] N. Yogesh, T. Fu, F. Lan, and Z. Ouyang, "Far-infrared circular polarization and polarization filtering based on Fermat's spiral chiral metamaterial," *IEEE Photon. J.*, vol. 7, no. 3, pp. 1–12, Jun. 2015.

[2] P. Fei, Z. Shen, X. Wen, and F. Nian, "A single-layer circular polarizer based on hybrid meander line and loop configuration," *IEEE Trans. Antennas Propag.*, vol. 63, no. 10, pp. 4609–4613, Oct. 2015.

[3] B.A. Munk, *Frequency-Selective Surfaces—Theory and Design*. New York, NY, USA: Wiley, 2000.

[4] L. Young, L. Robinson, and C. Hacking, "Meander-line polarizer," *IEEE Trans. Antennas Propag.*, vol. AP-21, no. 3, pp. 376–378, May 1973.

[5] R. Orr, G. Goussetis, V. Fusco, and E. Saenz, "Linear-to-circular polarization reflector with transmission band," *IEEE Trans. Antennas Propag.*, vol. 63, no. 5, pp. 1949–1956, May 2015.

[6] P. Naseri, S. A. Matos, J. R. Costa, C. A. Fernandes, and N. J. G. Fonseca, "Dual-band Dual-Linear-to-Circular polarization converter in transmission mode application to *K*/*Ka*-band satellite communications," *IEEE Trans. Antennas Propag.*, vol. 66, no. 12, pp. 7128–7137, Dec. 2018.

[7] Q. Zeng, W. Ren, H. Zhao, Z. Xue, and W. Li, "Dual-band transmission-type circular polariser based on frequency selective surfaces," *IET Microw., Antennas Propag.*, vol. 13, no. 2, pp. 216–222, Feb. 2019.

[8] H. Li, B. Li, and L. Zhu, "Wideband linear-to-circular polarizer based on orthogonally inserted slot-line structures," *IEEE Antennas Wireless Propag. Lett.*, vol. 18, no. 6, pp. 1169–1173, Jun. 2019.

[9] H. B. Wang and Y. J. Cheng, "Single-layer dual-band linear-to-circular polarization converter with wide axial ratio bandwidth and different polarization modes," *IEEE Trans. Antennas Propag.*, vol. 67, no. 6, pp. 4296–4301, Jun. 2019.

[10] H.-F. Zhang, L. Zeng, G.-B. Liu, and T. Huang, "Tunable linear-to-circular polarization converter using the graphene transmissive metasurface," *IEEE Access*, vol. 7, pp. 158634–158642, Nov. 2019.

[11] H.-T. Chen, A. J. Taylor, and N. Yu, "A review of metasurfaces: Physics and applications," *Rep. Prog. Phys.*, vol. 79, no. 7, Jul. 2016, Art. no. 076401.

[12] M. Akbari, M. Farahani, A.-R. Sebak, and T. A. Denidni, "Ka-band linear to circular polarization converter based on multilayer slab with broadband performance," *IEEE Access*, vol. 5, pp. 17927–17937, 2017.

[13] M. Hosseini and S. V. Hum, "A circuit-driven design methodology for a circular polarizer based on modified Jerusalem cross grids," *IEEE Trans. Antennas Propag.*, vol. 65, no. 10, pp. 5322–5331, Oct. 2017.

[14] W. Zhang, J.-Y. Li, and J. Xie, "A broadband circular polarizer based on cross-shaped composite frequency selective surfaces," *IEEE Trans. Antennas Propag.*, vol. 65, no. 10, pp. 5623–5627, Oct. 2017.

[15] C. Jin, Q. Lv, and R. Mittra, "Dual-polarized frequency-selective surface with two transmission zeros based on cascaded ground apertured annular ring resonators," *IEEE Trans. Antennas Propag.*, vol. 66, no. 8, pp. 4077–4085, Aug. 2018.

[16] D. Blanco and R. Sauleau, "Broadband and broad-angle multilayer polarizer based on hybrid optimization algorithm for low-cost ka-band applications," *IEEE Trans. Antennas Propag.*, vol. 66, no. 4, pp. 1874–1881, Apr. 2018.

[17] S. Khan and T. F. Eibert, "A dual-band metasheet for asymmetric microwave transmission with polarization conversion," *IEEE Access*, vol. 7, pp. 98045–98052, 2019.

[18] E. Arnieri, F. Greco, and G. Amendola, "A broadband, wide-angle scanning, linear-to-circular polarization converter based on standard jerusalem cross frequency selective surfaces," *IEEE Trans. Antennas Propag.*, vol. 69, no. 1, pp. 578–583, Jan. 2021.

[19] M. Euler, V. Fusco, R. Dickie, R. Cahill, and J. Verheggen, "Sub-mm wet etched linear to circular polarization FSS based polarization converters," *IEEE Trans. Antennas Propag.*, vol. 59, no. 8, pp. 3103–3106, Aug. 2011.
[20] J. D. Baena, S. B. Glybovski, J. P. del Risco, A. P. Slobozhanyuk, and P. A. Belov, "Broadband and thin linear-to-circular polarizers based on self-complementary zigzag metasurfaces," *IEEE Trans. Antennas Propag.*, vol. 65, no. 8, pp. 4124–4133, Aug. 2017.
[21] A. K. Fahad, C. Ruan, R. Nazir, M. Saleem, T. U. Haq, S. Ullah, and W. He, "Ultra-thin metasheet for dual-wide-band linear to circular polarization conversion with wide-angle performance," *IEEE Access*, vol. 8, pp. 163244–163254, 2020.
[22] M. Bakir, K. Delihacioglu, M. Karaaslan, F. Dincer, and C. Sabah, "U-shaped frequency selective surfaces for single- and dual-band applications together with absorber and sensor configurations," *IET Microw., Antennas Propag.*, vol. 10, no. 3, pp. 293–300, Feb. 2016.
[23] O. Turkmen, E. Ekmekci, and G. Turhan-Sayan, "Nested U-ring resonators: A novel multi-band metamaterial design in microwave region," *Microw., Antennas Propag., IET*, vol. 6, no. 10, pp. 1102–1108, Jul. 2012.
[24] Z. Li, R. Zhao, T. Koschny, M. Kafesaki, K. B. Alici, E. Colak, H. Caglayan, E. Ozbay, and C. M. Soukoulis, "Chiral metamaterials with negative refractive index based on four 'U' split ring resonators," *Appl. Phys. Lett.*, vol. 97, no. 8, 2010, Art. no. 081901.
[25] M. Mutlu, A. E. Akosman, A. E. Serebryannikov, and E. Ozbay, "Asymmetric chiral metamaterial circular polarizer based on four U-shaped split ring resonators," *Opt. Lett.*, vol. 36, no. 9, pp. 1653–1655, 2011.
[26] C. A. Balanis, *Antenna Theory: Analysis and Design*. Hoboken, NJ, USA: Wiley, 2016.
[27] I. S. Syed, Y. Ranga, L. Matekovits, K. P. Esselle, and S. G. Hay, "A single-layer frequency-selective surface for ultrawideband electromagnetic shielding," *IEEE Trans. Electromag. Compat.*, vol. 56, no. 6, pp. 1404–1410, Dec. 2014.
[28] D. Li, T.-W. Li, E.-P. Li, and Y.-J. Zhang, "A 2.5-D angularly stable frequency selective surface using via-based structure for 5G EMI shielding," *IEEE Trans. Electromagn. Compat.*, vol. 60, no. 3, pp. 768–775, Jun. 2018.
[29] L. Matekovits, A. De Sabata, and A.-M. Silaghi, "Frequency selective surface with two quasi-independent notch frequencies," *IEEE Access*, vol. 7, pp. 77261–77267, 2019.

ANDREI-MARIUS SILAGHI (Student Member, IEEE) received the B.Sc. degree in electronics and telecommunications, the M.Sc. degree in communication networks, and the Ph.D. degree from University Politehnica Timisoara, in 2013, 2015, and September 2019, respectively. He is currently a Research Assistant in electromagnetic compatibility, microwaves, antennas and wave propagation and electrical measurements with the Department of Measurements and Optical Electronics, University Politehnica Timisoara. He is also an EMC Design Consultancy and a Simulation Engineer with Continental Automotive, Timisoara. He published 44 articles in journals and conferences (2 in ISI journals, 25 in ISI indexed conferences, and 14 Scopus indexed conferences). The quality of his research is reflected from the 26 ISI Conferences citations, from which 3 were in ISI Q2 Journals.

ALDO DE SABATA (Member, IEEE) received the Ph.D. degree in electronics and telecommunications and the Habilitation degree in electronics and telecommunications in 1992 and 2013, respectively. He is currently a Full Professor with the Faculty of Electronics, Telecommunications and Information Technologies, University Politehnica Timisoara, and also a Coordinator of the Electromagnetic Compatibility Group (4 Ph.D. Students in the EMC area). He published more than 150 articles in journals and conferences and 7 books and conducted contracts and grants in the fields of: high frequency technique, electromagnetic compatibility, signal processing, and solar energy. His present research interests include metamaterials, metasurfaces, and rf spectrum measurement and modeling. His current teaching activity is related to microwaves, antennas and propagation, electromagnetic compatibility, and digital signal processing.

LADISLAU MATEKOVITS (Senior Member, IEEE) received the degree in electronic engineering from the Institutul Politehnic din Bucureşti, Bucureşti, Romania, in 1992, and the Ph.D. degree (Dottorato di Ricerca) in electronic engineering from the Politecnico di Torino, Turin, Italy, in 1995.

Since 1995, he has been with the Department of Electronics and Telecommunications, Politecnico di Torino, first with a Postdoctoral Fellowship, then as a Research Assistant. In 2002, he joined as an Assistant Professor with the Department of Electronics and Telecommunications and was appointed as a Senior Assistant Professor in 2005 and as an Associate Professor in 2014. In late 2005, he was a Visiting Scientist with the Antennas and Scattering Department, FGAN-FHR (now Fraunhofer Institute), Wachtberg, Germany. Beginning July 2009, for two years, he has been a Marie Curie Fellow with Macquarie University, Sydney, NSW, Australia, where he also held a visiting academic position in 2013 and has been appointed as an Honorary Fellow in 2014. In February 2017, he received the Full Professor qualification in Italy. Since 2020, he has been an Honorary Professor with University Politehnica Timisoara, Romania, and has also been an Associate of the National Research Council of Italy. He has also been appointed as a Member of the National Council for the Attestation of University Degrees, Diplomas and Certificates (CNATDCU), Romania, from 2020 to 2024. His current research interests include the concern numerical analysis of printed antennas and in particular development of new, numerically efficient full-wave techniques to analyze large arrays, optimization techniques, and active and passive metamaterials for cloaking applications. Material parameter retrieval of these structures by inverse methods and different optimization techniques has also been considered. In the last years, bio-electromagnetic aspects have also been contemplated, as for example design of implantable antennas or development of nano-antennas for example for drug delivery applications. He has published more than 375 articles, including more than 90 journal contributions, and delivered seminars on these topics all around the world: Europe, USA (AFRL/MIT-Boston), Australia, China, and Russia. He has been invited to serve as a Research Grant Assessor for government funding calls (Romania, Italy, Croatia, and Kazakhstan) and as an International Expert in Ph.D. thesis evaluation by several Universities from Australia, India, Pakistan, and Spain.

Dr. Matekovits has been a member of the Organizing Committee of the International Conference on Electromagnetics in Advanced Applications (ICEAA), since 2010. He is a member of the technical program committees of several conferences. He has been a recipient of various awards in international conferences, including the 1998 URSI Young Scientist Award (Thessaloniki, Greece), the Barzilai Award 1998 (young Scientist Award, granted every two years by the Italian National Electromagnetic Group), and the Best AP2000 Oral Paper on Antennas, and ESA-EUREL Millennium Conference on Antennas and Propagation, Davos, Switzerland. He was a recipient of the Motohisa Kanda Award 2018, for the most cited article of the IEEE TRANSACTIONS ON ELECTROMAGNETIC COMPATIBILITY (EMC) in the past five years, and more recently he has been awarded with the 2019 American Romanian Academy of Arts and Sciences (ARA) Medal of Excellence in Science and by the Ad Astra Award 2020, a Senior Researcher, for Excellence in Research. He has been an Assistant Chairman and a Publication Chairman of the European Microwave Week 2002, Milan, Italy, and has also been a General Chair of the 11^{th} International Conference on Body Area Networks (BodyNets) 2016. He serves as an Associate Editor for IEEE ACCESS, the IEEE ANTENNAS AND WIRELESS PROPAGATION LETTERS, and (MAP). He also serves as a reviewer for different journals.